Microwave-Assisted Synthesis and Physicochemical Characterization of Tetrafuranylporphyrin-Grafted Reduced-Graphene Oxide

Microwave-assisted synthesis and physico-chemical characterization of tetrafuranylporphyrin grafted reduced-graphene oxide

Federica Bosca,[a] Laura Orio,[a] Silvia Tagliapietra,[a] Ingrid Corazzari,[b] Francesco Turci,[b,d] Katia Martina,[a] Linda Pastero,[c,d] Giancarlo Cravotto[a] and Alessandro Barge*[a]

[a] Department of Drug Science and Technology, University of Turin, Via Giuria 9, 10125 Turin, Italy E-mail: alessandro.barge@unito.it
[b] Department of Chemistry, University of Turin, Via Giuria 9, 10125 Turin, Italy
[c] Department of Earth Sciences, University of Turin, Via Valperga Caluso 35, 10125 Turin, Italy
[d] Interdepartmental Center "G. Scansetti", University of Turin, Via P. Giuria 7, 10125 Turin (Italy)

Abstract: This work describes the design of a modified porphyrin which bears four furan rings linked by 1,2-bis-(2-aminoethoxy)-ethane spacers. This unit is a well suited scaffold for a Diels-Alder reaction with commercial reduced-graphene oxide, which is also described in this paper. A new hybrid material is obtained, thanks to efficient grafting under microwave irradiation, and fully characterized in terms of structure (UV, TGA, Raman) and morphology (HR-TEM and AFM). Potential applications in photo- and sonodynamic therapy are envisaged.

Their unique structure confers to carbon based nanomaterials particular physical and chemical properties that make them truly promising systems. Indeed, they have wide ranging applications in various fields, such as engineering, biology, chemistry, physics and medicine.[1-8]

Graphene is a single-atom-thick layer of graphite, which is prepared via a number of methods: mechanical, epitaxial, reduction of graphene oxide (GO) and solvent dispersion of graphite.[9] It is a nanomaterial characterized by extended π–conjugation which makes its manipulation difficult because of its tendency to aggregate. However, this peculiar aromaticity provides a suitable surface for combining graphene with other substrates.[10,11] Graphene, together with a number of other nanomaterials i.e. CNTs and fullerenes,[12] has attracted widespread attention for this reason. GO and reduced GO (rGO)[13] are two carbon nanomaterials which are direct graphene derivatives. These systems are characterized by oxygenated groups; rGO mainly bears these functional groups (OH, COOH) on its borders, meaning that the aromatic character of the planar carbon surface is almost completely maintained.[14-23] For these reasons, in this study, rGO has been selected as suitable substrate to be grafted with *ad hoc* synthesized porphyrin via Diels-Alder reaction. The aim of this chemical decoration is to realize an hybrid nanomaterial for potential application in photo- or sono-dynamic therapy[24,]. Indeed, both rGO planar surfaces can be exploited to accommodate many chemical structures and the residual functional groups offer the possibility of linking other suitable molecules,[25] thus improving their ability to be suspended and providing active targeting. Furthermore, the choice of rGO and this specific porphyrin conjugation may favour radical delocalization and stabilization. This latter effect is particularly relevant when these hybrid nanomaterials are employed in photo- or sono-dynamic therapies, as these applications require a photo- or a sono-sensitizing agent.[25-30]

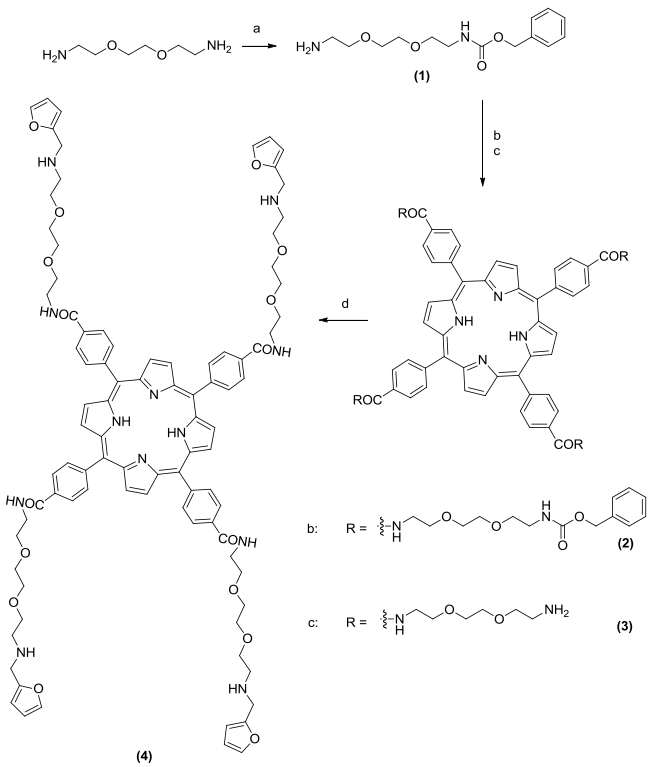

Scheme 1. Synthetic pathway for the furane modified porphyrin. a) benzyl chloroformiate, H_2O/EtOH/Dioxane, 0°C, pH=7; b) meso tetra-(4-carboxyphenyl)-porphyrin, EDC, DMAP, DCM; c) H_2, Pd/C, MeOH/Dioxane; d) furfural, $Na(AcO)_3BH$, MeOH, pH=5

Porphyrins are the candidate of choice here as they can be subjected to excitation by both light and ultrasound irradiation[24] while the production of radicals that occurs as a consequence of the relaxation phenomenon can induce cell death.[31,32]
We designed the structure of compound (**4**) (scheme 1) with the aim of generating a porphyrin-rGO based hybrid material with potential applications in photo- and sonodynamic therapy. The idea here is that (**4**) can be linked to rGO by more than one moiety, thus increasing the probability of the porphyrin orientating itself coplanar with the rGO surface and maintaining the original graphene sheet geometry (figure 1). In the same way, compound (**4**) could interpose itself between two rGO foils giving interesting multilayer structures. We selected the Diels Alder reaction because, unlike 1,3-dipolar cycloaddition, it does not require the *in situ* formation of a reactive intermediate. This peculiar behaviour is particularly suitable for simultaneous multi-point grafting. (figure 1)

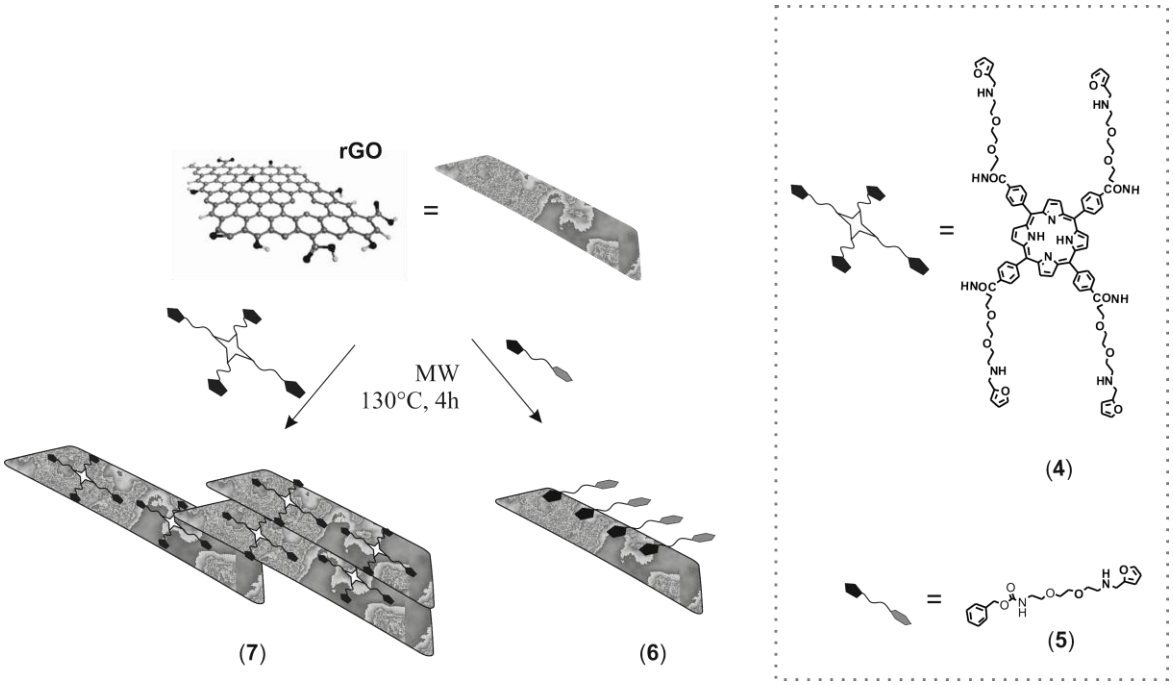

Figure 1. Synthetic scheme of rGO functionalization by Diels Alder reaction

Furan modified porphyrin (**4**) was obtained from the carboxybenzyl monoprotection of 1,2-bis-(2-aminoethoxy)-ethane (**1**) and then further conjugation to meso-tetra-(4-carboxyphenyl)-porphyrin to give product (**2**). The four amino-groups were then deprotected by hydrogenolysis to give (**3**) and the desired product (**4**) was obtained following reductive amination with furfural. The low solubility of (**4**) makes isolation very easy, while analytical characterization was a difficult affair.

The conditions for the Diels Alder reaction between commercial rGO (Sigma Aldrich) and furan modified porphyrin were optimized using compound (**5**) which can simulate the arm of final compound (**4**). The reaction was carried out under microwave (MW) irradiation in a monomode reactor (Anton Parr). Different reaction times, temperatures and molar ratios were explored. TGA analyses provided the optimal reaction conditions to obtain (**6)** (figure 1): 4 hours, 130°C and a (**5**)/rGO weight ratio of 1.2. MW irradiation strongly promoted the Diels-Alder cycloaddition[33] and in spite of reactive groups available for conjugation (carboxylic residues on rGO surface and hindered secondary amine on **5**) no side reactions could be detected. Typically the direct MW-assisted amidation with carboxylic acids and amines requires activators (e.g. HBTU, HATU, PyBOP, carbodiimides, etc) or at least suitable solid catalysts (TiO_2) [34].

In accordance with the conditions mentioned above, rGO was reacted with a DMF solution of (**4**) to give (**7**). The UV spectrum of (**7**) shows the characteristic Soret band which indicates the presence of porphyrin on the graphene surface. The red shift of this maximum peak (figure 2) is consistent with analogous observations that have already been reported in the literature [25-30].

The thermal behaviour of (**7**) was studied by TGA under nitrogen in the temperature range of 150-800 °C, and compared with that of both r-GO/(**4**) mixture and r-GO pristine (figure 3).

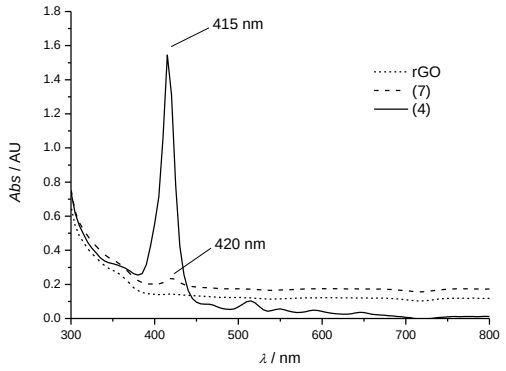

Figure 2. UV-Vis spectra of (**4**) (solid line), (**7**) (dashed line) and pristine rGO (dotted line) in DMF

In the temperature range of 150-270 °C (region **I**), (**7**) exhibited a mass loss which was significantly higher than that observed with both pristine rGO and the rGO/(**4**). This process was assigned, in part, to the thermal decomposition of residual labile functionalities (e.g. OH, COOH) from rGO structure and, in part, to the evolution of volatile contaminants deriving from the functionalization procedure

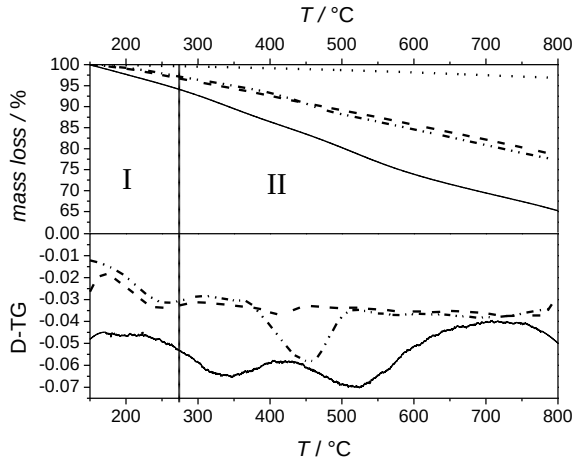

Figure 3. Upper panel: TGA analyses of pristine rGO (dashed line); (**7**) obtained after MW irradiation for 4h, 130°C, of (4)/rGO =1.2 (w/w) (solid line); rGO/(**4**) mixture of (dash dot dot). The thermal behaviour of carbon soot (dotted line) is reported to prove the inertness of the atmosphere inside the furnace during the heating ramp. Lower panel: derivative TG curves of pristine rGO (dashed line), rGO/(**4**) mixture (dash dot dot) and (**7**) (solid line).

In the temperature range of 271-800 °C (region **II**), (**7**) and rGO/(**4**) mixture underwent a mass loss of ca. 29% and 20%, respectively. In both cases, this datum was unequivocally ascribed to the thermal decomposition of (**4**) by comparison with pristine rGO. Comparing the D-TG curves evidenced the different nature of the interaction occurring between (**4**) and r-GO in the samples (**7**) and r-GO/(**4**), respectively. In particular the process occurring at the higher temperature (minimum peak at 520 °C) with (**7**) evidenced the presence of stronger interactions which were not observable with the simple mixture. This result further supports the successful formation of covalent bonds between porphyrin and rGO in (**7**).

Raman spectroscopy and high-resolution imaging techniques (TEM and AFM) have been carried out to evaluate the structural alterations that may possibly be induced on rGO during the functionalization.[35] Graphene has two main Raman-active bands; the in-phase vibration of the graphite lattice (G band) at ca. 1580 cm^{-1} and the so-called disorder band (D band) at ca. 1350 cm^{-1}. A D' band at ca. 1600 cm^{-1}, often overlapped with the G band, is observed when a sufficient number of defects are present in the carbon lattice (figure 4A, spectrum a). The 2D and 2D′ overtones and the D + G combination modes produce a large convoluted band at higher frequencies in the 2500-3500 cm^{-1} region. An increase in the relative Raman intensity of the D and D' bands, as compared to the G band, is generally observed when the disorder of graphite layers increases. A representative Raman spectrum of pristine rGO is reported in figure 4A (spectrum a). The significantly high defect content, which is indicated by the high relative intensity of the D band with respect to the G band, is consistent with a high number of sp3 carbons introduced during the oxidative preparation of the material and only partially reconverted to sp2 during the reduction step. The Raman spectrum recorded for (**7**) (figure. 4A, spectrum b) is very similar to that of pristine rGO. This indicates that the functionalization with (**4**) only slightly altered the rGO defect content. The average ID/IG ratio, a convenient parameter to estimate the overall defectiveness of graphitic materials, was calculated on several Raman spectra collected with rGO and (**7**). (figure 4B). The measured ID/IG ratio was 1.27 ± 0.04 and 1.09 ± 0.04 for pristine rGO and (**7**), respectively. The high ID/IG ratio (> 1) measured for pristine rGO may be explaned by a large number of polyaromatic domains with smaller overall size and the occurrence of patches with a highly defective carbon lattice that were induced by the oxidative processing of graphene.[36] The slight decrease in ID/IG ratio observed for the functionalized (**7**) sample clearly indicates that the adopted synthetic approach followed during the synthesis does not further modify the hybridization of C. The observed decrease may be caused by the thermal annealing of graphene defects assisted by MW irradiation [37].

A morphological analysis of rGO and (**7**) was carried out by means of high resolution microscopies, namely TEM and AFM. HR-TEM images of pristine rGO and of (**7**) are reported in figure 5, A and C respectively. The structure of the pristine rGO exhibits large exfoliated planes where porphyrin grafting may likely occur. The 2-D carbon sheets are occasionally terminated by wrinkles (white arrows) that indicate areas of higher material atomic density (darker portions in the bright field TEM image) and possibly contain a higher number of structural defects.

The AFM investigation of pristine rGO (figure 5, B) confirms the largely exfoliated nature of the sample by displaying the occurrence of several thin sheets (arrows) with well-defined geometry (dotted lines). The lateral extension of the aggregates ranges between 0.25 µm and 1 µm in pristine rGO. The pileup of graphene monolayers is thus confirmed by AFM measurements; sheet thickness distribution (fig. S13, in the Supporting material) ranges from 2.5 to 300 nm (between 7 and 870 monolayers if considering a theoretical monolayer thickness of 0.345 nm).

The nanoscale morphology of functionalized (**7**) remains largely unchanged with regards to pristine rGO. The slight increase in denser structures (dark areas) may account for an increase in piled graphene sheet thickness upon conjugation. This is compatible with the formation of intra-layer cross-linking bridges favoured by the presence of porphyrin. Graphene monolayers of regular shape and unaltered borders are still clearly visible (black arrows) both at TEM and AFM resolution. The AFM analysis of the sample reveals the existence of thin multi-layered structures with a regular outline. The lateral width of the structures in loaded samples is lower (0.5µm) than in the pristine form on average. At the same time, the thickness of the multilayer stacks decreases, ranging from 2.5 to 95 nm (7 to 275 theoretical monolayers). Despite the thickness value trend apparently being the opposite of what was expected, it can be explained by the increased stacking order that occurs as a consequence of functionalization. The occurrence of well-defined geometries is higher in the functionalized sample than in the pristine, meaning that the order in stacking increases is due to the development of intra-layer cross-linking bridges. On the other hand, the pile up of layers that arises in the pristine form derives from a chaotic superposition and folding of the layers.
The shape of a single-layer graphene sheet is preserved (dotted lines in Fig. 5 D) and a more isometric shape is reported in the aggregates (ca. 500 nm).

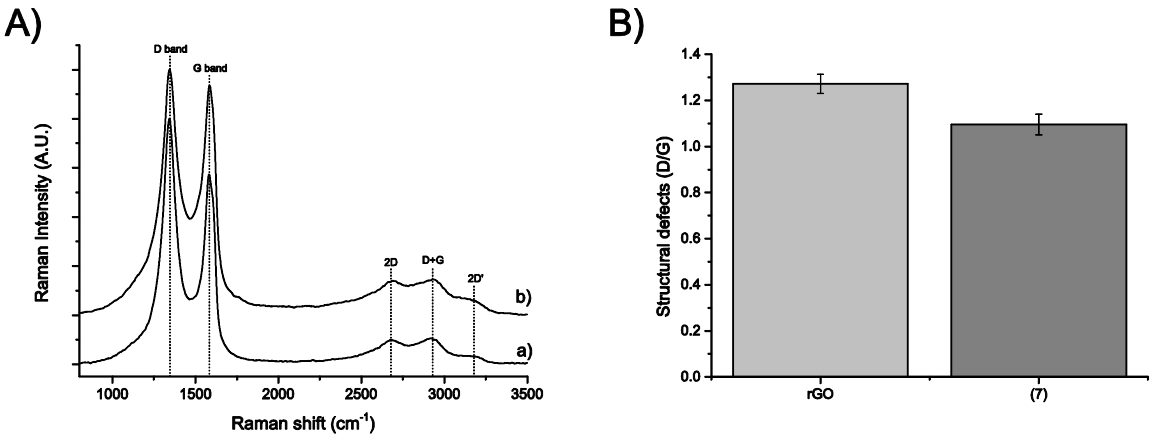

Figure 4. A) Raman spectra of rGO and (**7**) (spectra a and b, respectively), and B) evaluation of average graphene sheet defectiveness. All spectra were recorded with an exciting laser wavelength of 523 nm. The position of the G band peak is indicated by a vertical dashed line. The second-order Raman lines are also visible

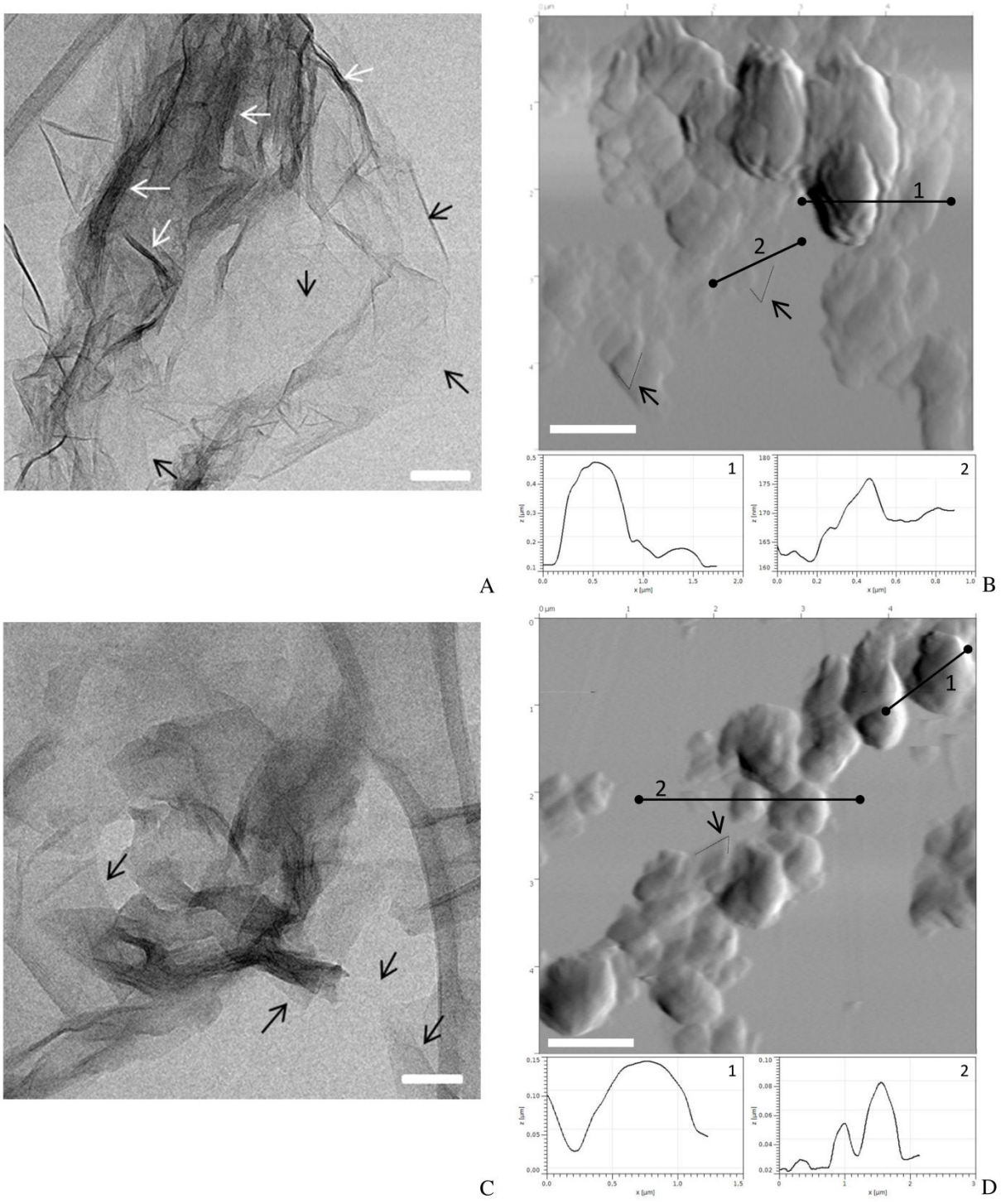

Figure 5. Representative images of pristine rGO (upper row) and (7) (lower row) as seen by TEM (A, C), and AFM (B, D). TEM images highlight the exfoliated flat morphology of the rGO sheets (black arrows) in which some denser material (white arrows), due to wrinkles in the graphene sheet, occasionally occurs. AFM images confirm the layered structure and the rhombohedral shape of the rGO sheets (black arrows). In order to improve the readability, amplitude images are reported. Some profiles are extracted to illustrate the height distribution. The thinner structures detectable have a minimum thickness of 2.5 nm (7 monolayers) in both cases. The thickness of the pile-up structures generally decreases in the loaded sample with respect to the pristine sample. Relative scale bar: 5 nm (TEM) and 1 μm (AFM).

In conclusion, we designed a four-arms star-shaped tetrafuranyl porphyrin, a platform well suited for an efficient multipoint covalent grafting with rGO. The MW-assisted graphene derivatization via Diels-Alder reaction with the porphyrin scaffold did not increase structural defects. The grafted material appears as a thin sheet with well-defined geometry, characterized by some multilayer cross-linked bridges. This peculiar connection forces the two structures in a “quasi” coplanar position. This is an interesting feature for photo- and sono-dynamic applications because of the easy delocalization of porphyrin-induced radicals by

π–π interactions on the whole graphene surface. An increased radicals half-life should also enhance the interaction of this material with biomolecular targets, a condition required for further development in nanomedicine cancer therapy.

.

Experimental Section

Materials and methods. All reagents and solvents were purchased from Sigma-Aldrich (Milan, Italy) and used without further purification unless specified, *meso*-tetrakis(4-carboxyphenyl)porphine was purchased from Frontier Scientific (Logan, Utah, USA). MW assisted reactions were carried out in a monomode reactor Monowave 300 (Anton Paar Italia Srl, Italy). TGA analyses were carried out under argon atmosphere on TGA 4000 (Perkin Elmer); TEM analyses on a JEOL 3010-UHR transmission electron microscope (TEM); micro-Raman spectroscopy on a confocal Raman microscope (Horiba Jobin-Yvon HR800 and Olympus BX41 microscope) and AFM measurements were performed using a DME SPM Microscope (DME Igloo, Denmark) equipped with a DS95-50E scanner (scan volume 50x50x5μm). More instrumental detail and syntheses of compounds **1-6** are reported in the supplementary information file.

Syntesis of *meso*-tetrakis-[4-(furan-2yl-methyl-aminoethoxy-ethoxyethyl-aminocarbonyl)-phenyl]-porphyrin grafted rGO (7). Compound (**4**) (93 mg, 0,057 mmol) was dissolved in DMF (2 mL) and the solution was put into a specific glass vial (10 mL volume) for Anton Parr MW reactor, together with a magnetic barr. rGO (15 mg) was then added, the vial was sealed with its pressure resistant cap and put in the MW cavity. Reaction mixture was heated under magnetic stirring at 130° for 4h. After cooling, the mixture was centrifuged and the solution separated from solid graphene. Solid was washed several times with DMF and finally with DCM, then it was dried at 80°C in an oven. Grafted rGO (**7**) was characterized by TGA, Raman spectroscopy, TEM and AFM imaging.

Acknowledgements

This research was supported by MIUR (fondi ricerca locale 2013) and Associazione Italiana per la Ricerca sul Cancro (MFAG 2012, MFAG-13048)

Keywords: reduced graphene oxide • graphene grafting • modified porphyrin • microwaves • Diels-Alder reaction

[1] Y. Zhu, S. Murali, W. Cai, X. Li, J.W. Suk, J.R. Potts, R.S. Ruoff, *Adv. Mater*. **2010,** 22, 3906-3924

[2] M.J. Allen, V.C. Tung, R.B. Kaner*, Chem. Rev*. **2010,** 110, 132-145

[3] Y. Dong, J. Li, L. Shi, J. Xu, X. Wang, Z. Guo, W. Liu, *J. Mater. Chem. A* 1 **2013,** 644-650

[4] Y. Yang, Y.M. Zhang, Y. Chen, D. Zhao, J.T. Chen, Y. Liu*, Chem. Eur. J.* **2012,** 18, 4208-4215

[5] C. Su, K.P. Loh, *Acc. Chem. Res.* **2013,** 46, 2275-2285

[6] W. Zhang, S. Wang, J. Ji, Y. Li, G. Zhang, F. Zhang, X. Fan, *Nanoscale* **2013,** 5, 6030-6033

[7] Z. Li, S. Wu, H. Ding, D. Zheng, J. Hu, X. Wang, Q. Huo, J. Guan, Q. Kan, *New J. Chem.* **2013**, 37, 1561-.

[8] A.B. Dongil, B. Bachiller-Baeza, A. Guerrero-Ruiz, I. Rodríguez-Ramos, *J. Cat.* **2011**, 282, 299-309.

[9] Songfeng Pei, Hui-Ming Cheng, *Carbon,* **2012,** 50, 3210-3228

[10] W. Song, C. He, W. Zhang, Y. Gao, Y. Yang, Y. Wu, Z. Chen, X. Li, Y. Dong, *Carbon,* **2014,** 77, 1020-1030

[11] X. Zhang, L. Hou, A. Cnossen, A. C. Coleman, O. Ivashenko, P. Rudolf, B. J. van Wees, W. R. Browne, B. L. Feringa, *Chem. Eur. J.,* **2011**, 17, 8957-8964

[12] L. Dai, D. W. Chang, J. Baek, W. Lu, *small*, **2012,** 8, 1130-1166

[13] a) M. M. Jaafar, G. P. M. K. Ciniciato, S. A. Ibrahim, S. M. Phang, K. Yunus, A. C. Fisher, M. Iwamoto, P. Vengadesh, *Langmuir,* **2015**, 31(38), 10426-10434; b) A. R. Akhiani,M. Mehrali, L. S. Tahan M. Mehrali,T. M. I. Mahlia, E. Sadeghinezhad, H. S. C. Metselaar, *J.Phys. Chem. C,* **2015,** 119(40), 22787-22796; c) H. Zhang, X. Bo, L. Guo, *Sensor. Actuat. B-Chem.,* **2015**, 220, 919-926.

[14] M. Acik, G. Lee, C. Mattevi, A. Pirkle, R. M. Wallace, M. Chhowalla, K. Cho, Y. Chabal, *J. Phys. Chem. C* **2011**, 115, 19761−19781.

[15] R. Larciprete, S. Fabris, T. Sun, P. Lacovig, A. Baraldi, S. Lizzit, *J. Am. Chem. Soc.* **2011**, 133, 17315−17321.

[16] S. Stankovich, D. A. Diki0.n, R. D. Piner, K. A. Kohlhaas, A. Kleinhammes, Y. Jia, Y. Wu, S. T. Nguyen, R. S. Ruoff, *Carbon* **2007**, 45, 1558−1565.

[17] C. Gomez-Navarro, R. T. Weitz, A. M. Bittner, M. Scolari, A. Mews, M. Burghard, K. Kern, *Nano Lett.* **2007**, 7, 3499−3503.

[18] Y. Shao, J. Wang, M. Engelhard, C. Wang, Y. Lin, *J. Mater. Chem.* **2010**, 20, 743−748.

[19] G. K. Ramesha, S. Sampath, *J. Phys. Chem. C* **2009**, 113, 7985−7989.

[20] G. Williams, B. Seger, P. V. Kamat, *ACS Nano* **2008**, 2, 1487−1491.

[21] Y. M. Shul'ga, V. N. Vasilets, S. A. Baskakov, V. E. Muradyan, E. A. Skryleva, Y. N. Parkhomenko, *High Energy Chem.* **2012**, 46, 117−121.

[22] L. Guardia, S. Villar-Rodil, J. I. Paredes, R. Rozada, A. Martinez-Alonso, J. M. D. Tascon, *Carbon* **2012**, 50, 1014−1024.

[23] A. Mathkar, D. Tozier, P. Cox, P. Ong, C. Galande, K. Balakrishnan, A. Leela Mohana Reddy, P. M. Ajayan, *J. Phys. Chem. Lett.* **2012**, 3, 986−991.

[24] a) W.M. Sharman, C.M. Allen, J.E. van Lier, *Drug Discov. Today*, **1999,** 4, 507– 517; b) I. Rosenthal, J. Z. Sostaric, P. Riesz, *Ultrason. Sonochem*., **2004**, 11, 349-363

[25] M. Zhang, B., Yuan, S. Kang, L. Qin, G. Li and X. Li, *RSC Adv*., 2015,

[26] H. Chen, X. Zhou, Y. Gao, B. Zheng, F. Tang, J. Huang, *Drug Discov. Today*, **2014**, 19, 502-509

[27] E. S. Nyman, P. H. Hynninen, *J. Photochem. Photobiol. B Biol*., **2004**, 73, 1-28

[28] S. Hilderbr, R. Weissleder, *Curr. Opin. Chem. Biol*., **2010**, 14, 71-79

[29] W. W. L. Chin , W. K. O. Lau, R. Bhuvaneswari, P. W. S. Heng , M. Olivo, *Cancer Lett*, **2007**, 245, 127-133

[30] K. Berg, P. K. Selbo, A. Weyergang, A. Dietze, L. Pransmickaite , A. Bonsted, *J. Microsc*, **2005**, 218, 133-147

[31] M. Kuroki, K. Hachimine, H. Abe, H. Shibaguchi, M. Kuroki, S. Maekawa, J. Yanagisawa, T. Kinugasa, T. Tanaka , Y. Yamashita, *Anticancer Res.,* **2007**, 27, 3673-3678

[32] L. B. Josefsen , R. W. Boyle, *Theranostics*, **2012**, 2, 916-966

[33] a) H. M. T. Albuquerque, C. M. M. Santos, J. A. S. Cavaleiro, A. M. S. Silva, *Eur. J. Org. Chem*. **2015**, 4732–4743; b) A. M. Sarotti, P. L. Pisano, S. C. Pellegrinet, *Org. Biomol. Chem.*, **2010**, 8, 5069–5073; c) M. Sridhar, K. L. Krishna, J. M. Rao, *Tetrahedron*, **2000**, 56, 3539–3545

[34] E. Calcio Gaudino, D. Carnaroglio, M. Gonçalves, L. Schmidt, G. M. Martra, C. Deiana, G. Cravotto, *Cat. Sci. Technol*., **2014**, 4(5), 1395-1399

[35] M. A. Pimenta, G. Dresselhaus, M. S. Dresselhaus, L. G. Cancado, A. Jorio, R. Saito., *Phys. Chem. Chem. Phys*., **2007**, 9, 1276–1291

[36] N. Wu, X. She, D. Yang, X. Wu, F. Su, Y. Chen, *J. Mater. Chem.,* **2012**, 22, 17254-17261

[37] Chen W., Yan L., Bangal P. R., *Carbon*, **2010**, 48, 1146–1152.